

Italian residential gas demand forecasting

Andrea Marziali^{1,2}, Emanuele Fabbiani², and Giuseppe De Nicolao²

¹Modelling and pricing, A2A

²Department of Electrical, Computer and Biomedical Engineering,
University of Pavia

29th June 2022

Abstract

Natural gas is one of the most important energy sources in Italy: it fuels thermoelectric power plants, industrial facilities and domestic heating. Forecasting gas demand is a critical process for each energy provider, as it enables pipe reservation and stock planning. In this paper, we address the problem of short-term forecasting of residential gas demand, by comparing several statistical learning models, including Ridge Regression, Gaussian Processes, and Deep Neural Networks. We also present the preliminary steps of preprocessing and feature engineering. To the best of our knowledge, no benchmark is available for the task we performed, thus we derive a theoretical performance limit, based on the inaccuracy of meteorological forecasts. Our best model, a deep neural network, achieves an RMSE which is about double with respect to the performance limit.

Keywords— natural gas; time series forecasting; statistical learning; Gaussian processes; neural networks

1 Introduction

In Italy, natural gas is the most common fuel for both power plants and domestic heating. Moreover, several industrial facilities burn gas for both heating and powering productive processes. According to SNAM, the Italian Transmission System Operator (TSO), in 2017 about 74.6 billions of cubic meters of natural gas were consumed, with an increase of 5.6% over the previous year. Overall, the increase in demand between 2014 and 2017 was 24%. A report published by the Economic Development Ministry shows that 33.8% of the gas demand in 2017 came from thermoelectric power plants, 19.2% from industrial facilities and the remaining 57% from residential users.

In this paper, we focus on the Italian residential gas demand (RGD), the largest portion of the total demand. Forecasting natural gas demand is a key task for each energy company for several reasons. Demand forecast provides relevant information to effectively reserve pipe capacity and to plan stocks. Furthermore, energy regulations impose the balance of the network by charging providers with a fee proportional to their unbalanced quantity. Finally, demand is a critical input to forecast gas price, which is in turn key for several business decisions.

The literature about gas demand forecasting is quite large: comprehensive reviews are [13] and [14]. According to Sebalj et al, papers can be classified by four aspects. The *prediction horizon* can range from hourly to yearly, the *reference area* from single nodes of the network to a whole country; adopted *models* include time series, mathematical and statistical approaches, neural networks (ANN) and others; input *features* can be demand history, temperature, calendar and other minor ones.

Focusing on country-level daily forecasts, mathematical and statistical models obtained by composing parametric non-linear functions are used in [3] to explain the factors which affect the demand. A different multi-factor approach is developed in [11] and a model based on the physical relation between gas demand and temperature is presented in [5]. An adaptive network-based fuzzy inference system (ANFIS) is described in [2], where the authors show the better performances of their model with respect to ANN and conventional time series methods. A statistical learning model, based on support vector machine (SVM), is developed in [19] to forecast UK demand, and compared with ANN and an autoregressive moving average (ARMA). A hybrid model, exploiting many different techniques such as wavelet transform, genetic algorithm, ANFIS and ANN is used in [10].

Neural networks are also applied in [17, 4, 16, 15, 18] to perform hourly and daily forecast on cities and regions.

To the best of our knowledge, no study about the Italian RGD has been published yet. Because of the lack of benchmarks, before addressing the forecasting problem, we developed a performance limit based on the inaccuracy of weather forecasts, a critical input for any Italian RGD model. Then, we present the key steps of preprocessing and feature engineering, devoting special attention to the identification of similar days and the transformation of temperature measures. The resulting dataset is the input of five statistical learning models: Ridge Regression, Gaussian Processes (GP), Nearest Neighbours (KNN), Deep Neural Networks (ANN) and a toroidal model previously applied to power load forecasting. An automatic procedure to optimize hyperparameters is applied to all of them, in order to maximize generalization capability. We found that GP and ANN achieve the best performances, with an RMSE about double the performance limit.

The paper is organized as follows. In section 2, we present the series of the RGD, highlighting its most important features. In section 3, we provide a statistical characterization of target and input variables and we present preprocessing and feature

engineering. Section 4 describes models, training process and hyperparameter tuning, providing some insight about the implementation. In section 5 we derive the performance limit, which is used as the ultimate benchmark in Section 6, where the results are presented and discussed. Finally, Section 7 is devoted to concluding remarks and possible future developments.

2 Problem Statement

The task addressed in this paper is the one-day-ahead forecasting of daily Italian RGD. Residential demand represents the main part of the overall Italian gas consumption, accounting for household usage for cooking, water heating and, most importantly, environment heating.

Available data cover 11 years, from 2007 to 2017 and are made of 3 fields: date (t), forecasted average temperature (T) and residential gas demand (RGD).

Forecasted temperature is provided by Meteologica, a well-known service, and is relative to the Northern regions of Italy. In the preliminary analysis, we also took into consideration a weighted average of the temperatures in different zones of Italy, but we noticed a weaker correlation with RGD. This is easily explainable with the larger use of domestic heating required by the colder winters of Northern Italy. The profile of RGD from 2007 to 2017 is displayed in Figure 1.

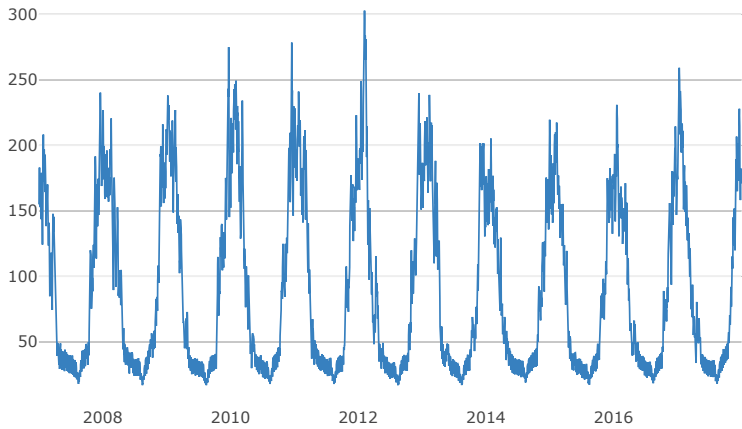


Figure 1: Italian Residential Gas Demand (RGD): years 2007-2017

3 Exploratory analysis and feature selection

3.1 Residential Gas Demand

RGD magnitude greatly oscillates with the season: during the cold months, from October to March, it represents about 56% of the Italian demand, while it drops to about 28% during the warm months, from April to Septembers. In fact, when the temperature climbs above 17-18 Celsius degrees, domestic heating gets typically switched off. Thus, during the cold period lower temperatures cause a larger RGD, while, during summer, weather influence is negligible. Instead, a seasonal pattern becomes evident, where weekends show lower RGD than working days. Due to the lack of dependence on weather conditions, RGD shows a lower variability across different years in summer than in the rest of the year. All these features are clearly visible in Fig. 2, which displays eleven years of Italian RGD, overlapped with a proper shift to align weekdays.

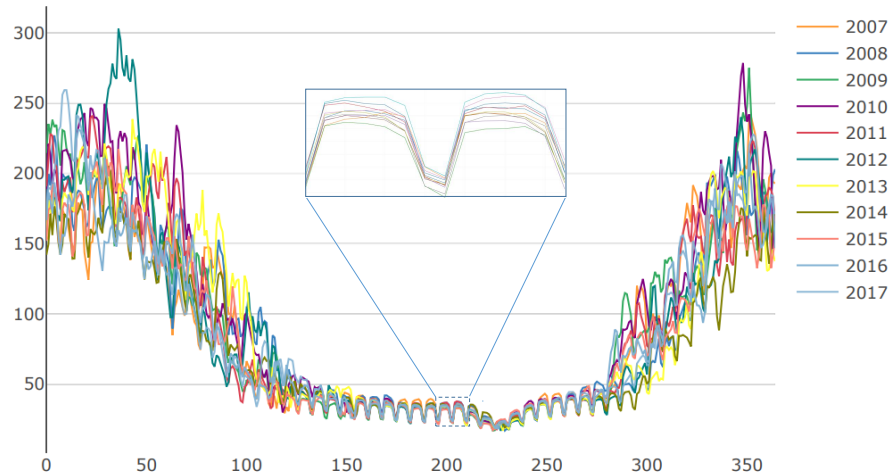


Figure 2: Italian Residential Gas Demand (RGD): years 2007-2017. The time series is shifted to align weekdays: weekly periodicity is particularly visible in summer. The yearly seasonality is mostly explained by heating requirements. In the inset, two weeks of July's demand data are zoomed.

To confirm the hints of visual inspection and uncover possible minor seasonal patterns, we resorted to autocorrelation and spectral density, depicted in Fig. 3 and Fig. 4. Both plots highlight a dominant yearly periodicity. In the spectral density it corresponds to harmonics whose frequencies are multiple of 1/year, with the largest spectral peak at 1/year and the second largest one at 2/year - note that, in order to account for leap years, 1 year = 365.25 days. There is also a smaller peak at frequency 52.18/year, i.e. 1/week, ascribable to the weekly periodicity.

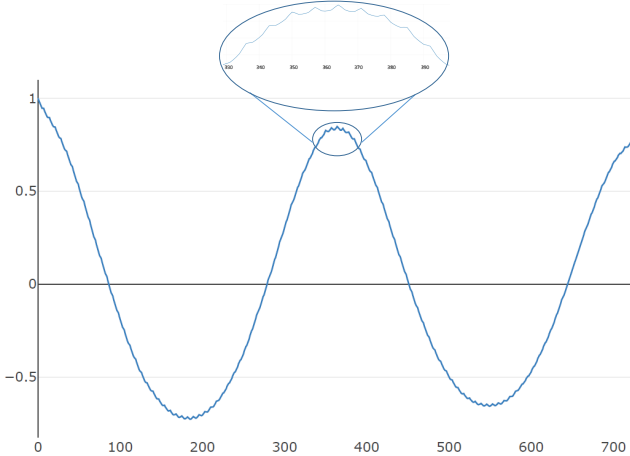


Figure 3: Residential gas demand: estimated autocorrelation function. The yearly periodicity is evident. In the inset, weekly waves witness the presence of a weekly periodicity of much smaller amplitude.

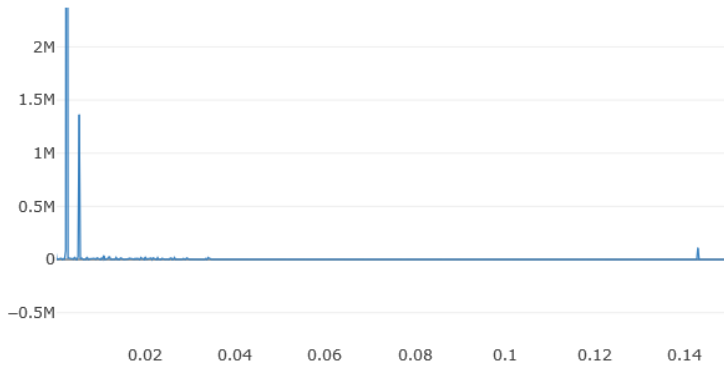


Figure 4: Residential gas consumption spectral density. The same considerations presented for autocorrelation hold: the yearly periodicity is highlighted by the peak at frequency $1/356.25$, while the weekly one by the smaller spike at frequency $1/7$. In order to reach a better representation, in the figure we cut off the highest yearly peak.

Notably, RGD shows a strong first order autoregressive behavior. To better appreciate the autocorrelation of lag 1, one can consider the scatter plots in Fig. 5a, where RGD at time t is plotted against RGD at time $t - 1$. The correlation coefficient computed on the entire dataset is 0.988, and it increases to 0.995 if Saturdays and Mondays

are discarded. This is an evidence of a different behavior between working days and weekends, visually confirmed in the plot, where Monday's RGD (orange dots) stays in the upper part of the cloud whereas Saturday's RGD (green dots) lies in the lower part.

Following the hints of the autocorrelation function, we examine also the relationship between RGD at time t and time $t - 7$. The scatter plot 5b is tighter when the demand is low - that is during cold months - while it gets more disperse when the demand is high. This is due to the influence of weather factors, which is larger when the temperature is lower.

More attention should be paid to the yearly seasonality, as it gets distorted by the misalignment of weekdays between consecutive years and the presence of holidays. To take this issues into account, we introduce the concept of similar day.

Definition 1 (Similar Day). *Given a day t , we define its similar day $sim(t)$ as the closest date of the previous year, in terms of calendar position, which respects the following constraints:*

- if t is not a holiday, $sim(t)$ is the same day of the week as t
- if t is not a holiday, $sim(t)$ is not a holiday
- if t is a holiday, $sim(t)$ is a holiday

According to the Italian calendar, holidays are: 1 January, 6 January, 25 April, 1 May, 2 June, 15 August, 1 November, 8, 25 and 26 December, Easter and Easter Monday.

The relationship between RGD and RGD in the similar day is shown in Fig. 5c: again, the correlation is higher when the demand is lower, due to the minor influence of exogenous factors, such as temperature.

It can also be of some interest to take into account the similar day of $t - 1$, as the difference between RGD at time $sim(t - 1)$ and RGD at time $sim(t)$ can be a proxy to the difference between RGD at time $t - 1$ and RGD at time t . The scatter plot in Fig. 5d confirms this hypothesis, as all the points are close to the 45-degree line.

Due to these considerations, we use RGD at times $t - 1$, $t - 7$, $sim(t)$ and $sim(t - 1)$ as inputs to forecast RGD at time t .

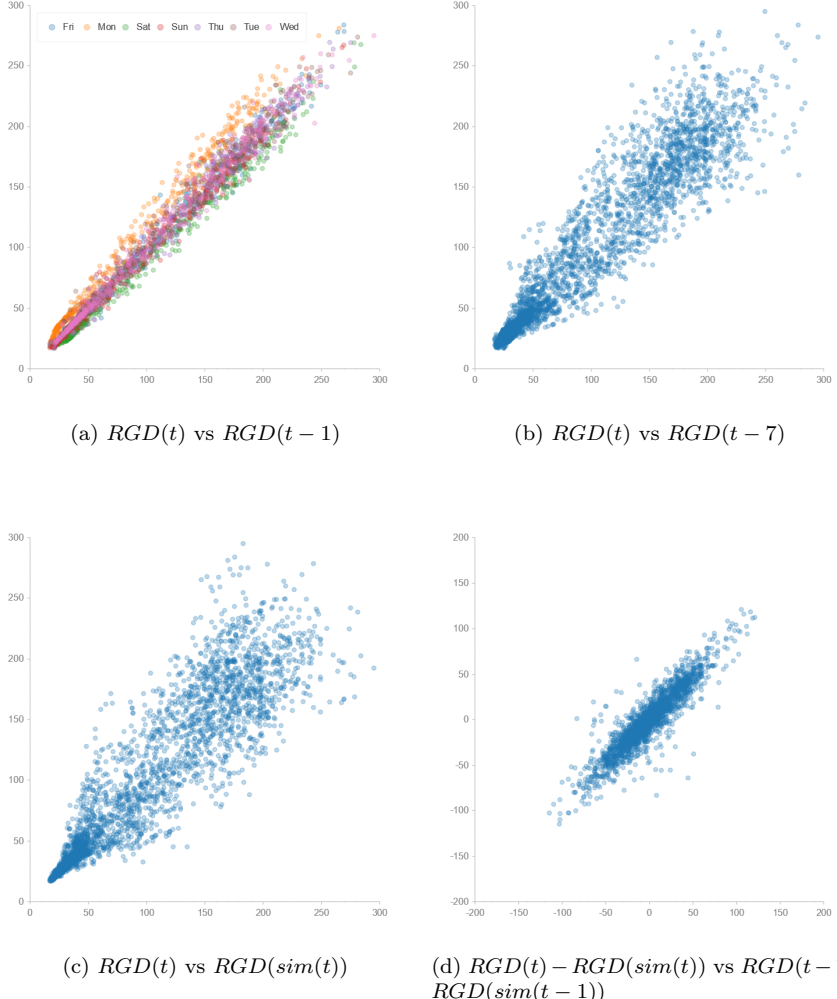


Figure 5: Scatter plots between features derived from RGD. Charts show how $RGD(t)$, $RGD(t-1)$ and $RGD(t-7)$ are positively correlated, more tightly when the demand is low, that is in warm months.

3.2 Temperature

The RGD time series shows a strong relationship with temperature, especially when, during the winter season, temperature falls below 18°C and household heating becomes relevant. As shown in the left panel of Fig. 6, the relationship is piecewise linear: a line with negative slope below 18°C , followed by an approximately constant line above 18°C . In order to transform the piecewise linear dependence into a linear one, it is useful to make reference to the so-called Heating Day Degrees (HDD):

Definition 2 (Heating Day Degrees (HDD)).

$$\text{HDD} = \max(18^\circ - T, 0) \quad (1)$$

In the right panel of Fig. 6, the scatter plot of RGD vs HDD highlights an approximately linear relationship, with a positive correlation of 0.97. The correlation of HDD with RGD is even more evident when we look at the time series of RGD and HDD (Fig. 7).

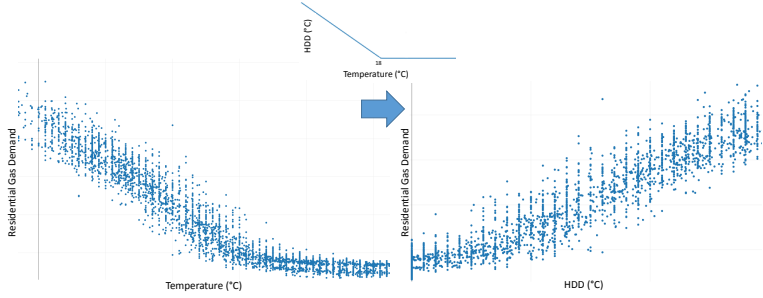


Figure 6: Left panel: scatter plot of daily RGD vs average daily temperature. Right panel: scatter plot of daily RGD vs HDD. Inset: HDD as a function of the temperature.

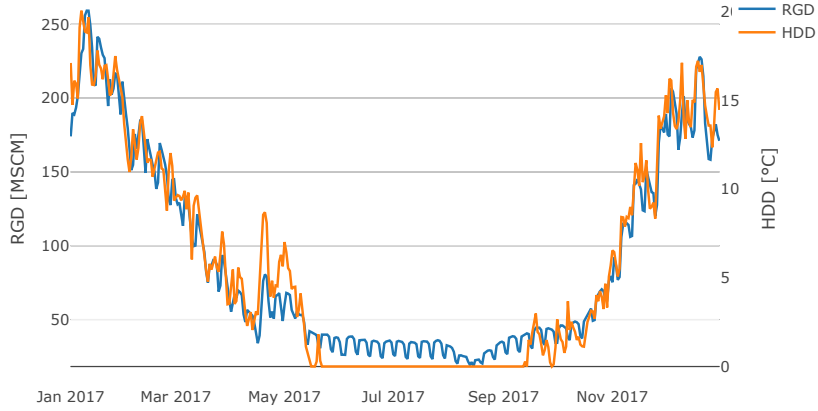


Figure 7: Time series of RGD and HDD in 2017. We can see a strong correlation between the two variables.

In order to predict $RGD(t)$, the forecasted temperatures at time t , $t - 1$, $t - 7$, $sim(t)$ are considered. However, as shown in Fig. 6, HDD are more correlated to gas demand

Feature	Reference time	Type
RGD	t-1	continuous
RGD	t-7	continuous
RGD	sim(t)	continuous
RGD	sim(t-1)	continuous
Forecasted temperature	t	continuous
Forecasted temperature	t-1	continuous
Forecasted temperature	t-7	continuous
Forecasted temperature	sim(t)	continuous
Forecasted HDD	t	continuous
Forecasted HDD	t-1	continuous
Forecasted HDD	t-7	continuous
Forecasted HDD	sim(t)	continuous
Weekday	t	categorical
Holiday	t	dummy
Day after holiday	t	dummy
Bridge holiday	t	dummy

Table 1: Features

than plain temperatures. Thus, we consider as inputs also predicted HDD at time t , $t - 1$, $t - 7$ and $sim(t)$

3.3 Calendar features

As shown in the previous paragraphs, weekdays and holidays have a great influence on RGD. To capture this phenomena, we add categorical calendar features.

Weekday. In view of the weekly periodicity, the seven days of the week are taken as explanatory features. By resorting to the one-hot encoding method they are transformed in n dichotomic time series with $n = 7$.

Holiday. A binary feature which takes value 1 in correspondence of holidays.

Day after holiday. A binary feature which takes value 1 the first working day after a holiday. A working day is a day different from Saturday or Sunday that is not a holiday.

Bridge holiday. A binary feature which takes value 1 on isolated working days, that is working days where both the day before and the day after are either Saturdays, Sundays or holidays.

3.4 Feature summary

To summarize, all the features are listed in Table 1

4 Models and their implementation

The classical methods used for time series forecasting are linear Box-Jenkins models such as *SARIMA*, where the forecast is based only on past values of the time series, and *SARIMAX*, that accounts also for exogenous variables. A major drawback of classical linear models is given by discontinuities due to holidays and the possible presence of other nonlinear phenomena. In order to overcome these difficulties, herein RGD forecasting is cast as a statistical learning problem.

Let y be our target variable and \mathbf{x} the vector of input features. Then, there exists a probability distribution $p(\mathbf{x}, y)$, from which all the samples (\mathbf{x}_i, y_i) are drawn. Based on n data pairs (\mathbf{x}_i, y_i) , $i = 1, \dots, n$, known as the training data, we design a prediction rule \hat{f} , such that $y \sim \hat{f}(\mathbf{x})$, by minimizing the empirical risk computed on a proper loss function. Then, we evaluate the goodness of our prediction model \hat{f} on another set of samples (\mathbf{x}_k, y_k) , $k = 1, \dots, m$, known as test set, using proper metrics.

In our context, $y = RGD$ and $\mathbf{x} \in \mathbb{R}^{22}$ is the vector made of the 22 features discussed in the previous section and shown in Table 1. In the following, with reference to the training data, $\mathbf{y} = \{y_i\} \in \mathbb{R}^n$ will denote the vector of the targets and $\mathbf{X} = \{x_{ij}\} \in \mathbb{R}^{n \times p}$ will denote the matrix of the inputs, where x_{ij} is the j -th feature of the i -th training pair (\mathbf{x}_i, y_i) .

Below, five approaches are illustrated: a regularized linear model, ridge regression; a linear model based on sinusoidal basis functions, toroidal model [7]; a non-parametric model, Gaussian processes (GP) and two non-linear models, k-nearest neighbour (KNN) and artificial neural networks (ANN).

4.1 Ridge regression

Ridge regression [8] is a technique to select a linear model in the form:

$$\hat{f}(\mathbf{x}) = \sum_{j=1}^p x_{ij} \beta_j = \mathbf{X} \boldsymbol{\beta}, \quad \boldsymbol{\beta} \in \mathbb{R}^p$$

To prevent overfitting, the loss function includes the square of the norm of the parameter vector $\boldsymbol{\beta}$ besides the standard squared sum of the residuals:

$$\boldsymbol{\beta}^{Ridge} := \arg \min_{\boldsymbol{\beta}} \|\mathbf{y} - \mathbf{X} \boldsymbol{\beta}\|^2 + \lambda \|\boldsymbol{\beta}\|^2 \quad (2)$$

where λ is the regularization parameter. The solution of (2) is

$$\boldsymbol{\beta}^{Ridge} = (\mathbf{X}^T \mathbf{X} + \lambda \mathbf{I})^{-1} \mathbf{X}^T \mathbf{y} \quad (3)$$

that highlights the shrinking effect introduced by the ridge regression with respect to the standard least squares estimator $\boldsymbol{\beta}^{LS} = (\mathbf{X}^T \mathbf{X})^{-1} \mathbf{X}^T \mathbf{y}$.

An alternative yet equivalent way of defining ridge regression is adding an inequality constraint to the loss function of a least square regression. A graphical interpretation of this definition is provided by Fig. 8.

$$\begin{cases} \boldsymbol{\beta}^{Ridge} = \operatorname{argmin}_{\boldsymbol{\beta}} \sum_{i=1}^N (y_i - \sum_{j=1}^p x_{ij} \beta_j)^2 \\ \sum_{j=1}^p \beta_j^2 \leq t \end{cases}$$

It can be shown that the hyperparameters λ and t are univocally linked.

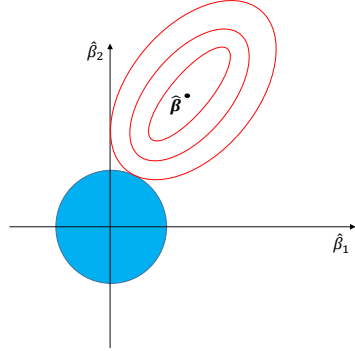


Figure 8: Ridge regression in a bidimensional space: the sum of the squared parameters can't be greater than the radius of the circle squared, the hyperparameter of the model.

The ridge regression model is completely defined once λ is chosen, as the parameters can be obtained in closed form (3).

We tune the hyperparameter λ by performing a line search on a wide set of possible values, using a 5-fold cross validation on the training set.

4.2 Gaussian processes

A Gaussian process (GP) [12, 9] is a stochastic process such that each random extraction of a finite number of points has a joint Gaussian distribution. We can model \hat{f} as a GP:

$$\hat{f}(x) \sim GP(m(x), k(x, x'))$$

with

$$\begin{aligned} m(x) &= \mathbb{E}[\hat{f}(x)] \\ k(x, x') &= \mathbb{E}[(\hat{f}(x) - m(x))(\hat{f}(x') - m(x'))^T] \end{aligned}$$

so that $m(x)$ is the mean and $k(x, x')$ is the covariance of a Gaussian distribution over functions.

The main distinctive feature of GP models is the learning process, which aims at building the predictive function rather than inferring its parameters. In terms of Bayesian inference, we can see the choice of the possible functions as a prior. Once evaluated the likelihood on a sample of data, it's possible to calculate the posterior probability to obtain a new observation y_* given a new set of features \mathbf{x}_*

$$p(y_* | \mathbf{x}_*, \mathbf{X}, \mathbf{y}) = \int p(y_* | \hat{f}, \mathbf{x}_*) p(\hat{f} | \mathbf{X}, \mathbf{y}) d\hat{f}$$

where the prior distribution $p(\hat{f}(x_1), \dots, \hat{f}(x_n))$ is jointly Gaussian for each set of points x_1, \dots, x_n and \hat{f} is a GP so that

$$p(\hat{f} | \mathbf{X}, \mathbf{y}) = \mathcal{N}(\boldsymbol{\mu}, \mathbf{K})$$

where $\boldsymbol{\mu} = (m(x_1), \dots, m(x_N))$ and $K_{ij} = k(x_i, x_j)$.

Often the mean of a GP is neglected as it only represents a translation. Thus, the GP is completely defined by his covariance function \mathbf{K} , also called kernel. If the covariance is stationary and isotropic, it becomes a function of a single argument r which is the distance between two points x_i and x_j .

In order to choose the covariance function, we tested several different possibilities provided by the literature [12]. By cross-validation, we selected a GP with a stationary and isotropic kernel given by the sum of Matérn and White functions.

Matérn is a general class of stationary and isotropic kernels defined by

$$k_{Matern}(r) = \frac{2^{1-\nu}}{\Gamma(\nu)} \left(\frac{\sqrt{2\nu}r}{l} \right)^\nu K_\nu \left(\frac{\sqrt{2\nu}r}{l} \right)$$

where ν and l are hyperparameters to be optimized and K_ν is a modified Bessel function [1]. The parameter l defines the characteristic length-scale of the process, whereas ν defines the specific covariance function in the Matérn class. If ν tends towards infinity, the Matérn formula reduces to the widely used squared exponential function

$$k_{SE}(r) = \exp\left(-\frac{r^2}{2l^2}\right)$$

while if $\nu = 1/2$ it becomes an exponential function

$$k_{EXP}(r) = \exp\left(-\frac{r}{l}\right)$$

The choice Matérn functions aims at modelling non-linear relationships between target variable and input features, while White kernels explain the noisy component of the gas demand.

Following the Bayesian interpretation of GPs, we adopted marginal likelihood maximization in order to choose hyperparameters.

4.3 K-Nearest neighbours

K-Nearest neighbours (KNN) is arguably the simplest non-linear model. KNN relies on the distance between samples in the feature space: given a test sample \mathbf{x}_* , the prediction of y_* is computed by averaging training samples $y_i, i = 1 \dots K$, corresponding to the K closest \mathbf{x}_i to \mathbf{x}_* , according to some distance measure.

The hyperparameters of KNN are three: the measure metric, the type of average, and K , the number of neighbours to consider. Considering small values of K leads to overfitting to the training data, while opting for including too many neighbours prevent the model from taking advantage by the information in the features. We resorted to a grid search with a 5-fold cross validation to appropriately choose K and the type of weight to use in the average.

4.4 Neural Networks

Artificial Neural Networks (ANN) are complex non-linear models, which trade explainability with the capability of capturing non-linear patterns and relationships. A comprehensive explanation of their structure and the most common training algorithms can be found in [6].

In this study, we focused on the simplest type of ANN, called Multi-Layer Perceptron (MLP) or fully connected ANN. We selected an architecture with one input layer of 24 neurons, two hidden layers of 12 and 4 neurons, and an output neuron of a single neuron, as shown in Fig. 9.

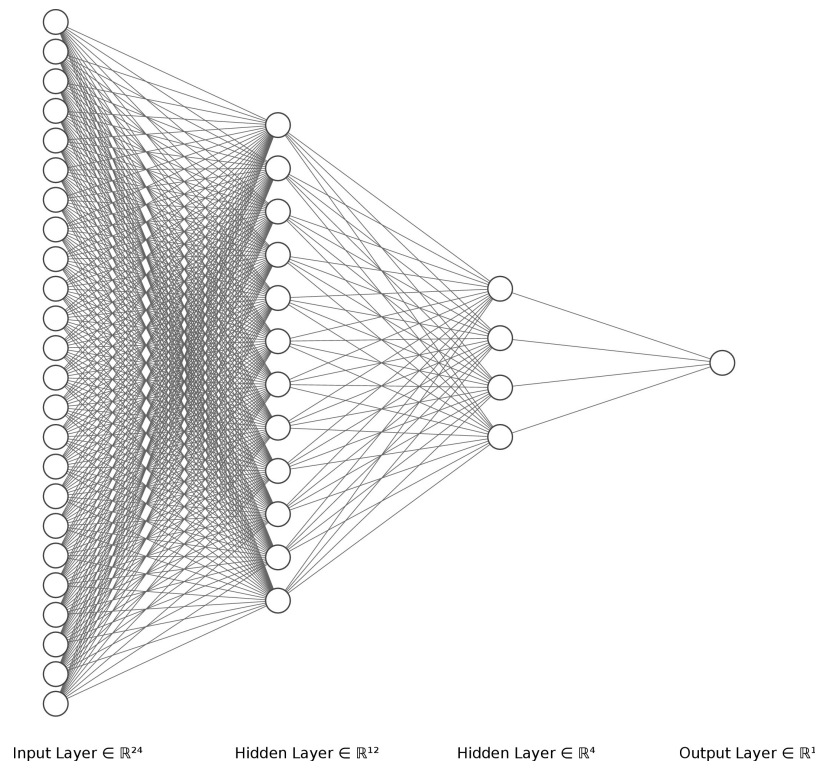


Figure 9: The ANN with 22 input features, three dense layers of 24, 12 and 4 neurons and an output neuron.

Beyond the architecture, there are many hyperparameters to optimize in order to enhance the performances, including the number of neurons in each layer, the activation functions, the optimization algorithm and its own parameters, such as number of epochs, batch size, loss function and learning rate.

We selected architecture, optimization algorithm and activation function by trials and

errors, while we used a grid search with 5-fold cross-validation to tune the learning rate, the batch size and the number of training epochs.

4.5 Toroidal model

The toroidal model [7] is a linear model based on sinusoidal functions, originally developed to predict power load. In this paper we adapt its short-term version to forecast RGD.

Following the approach of the authors, we first perform a logarithmic transformation of the RGD, to mitigate the effect of its skewness, then we develop a long term model

$$R\hat{G}D^{long}(t) = \exp(L(t) + F(t) + \sum_i H_i(t))$$

where the forecast of RGD is given by the exponential of the sum of three elements: the trend or level L , the potential F , which accounts for seasonality, and the effect of holidays $\sum_i H_i$. The exponential is a consequence of the logarithmic transformation of RGD.

The potential F is modelled by a linear combination of sinusoidal functions:

$$F(t) = \sum_{i=1}^{(1+2N_d)(1+2N_w)} \theta_i h_i(t), \quad \{h_i(t)\} = \mathcal{D} \otimes \mathcal{W}$$

where the functions h_i are given by the product of the j -th element in \mathcal{D} with the k -th element in \mathcal{W} , for suitable j and k , and

$$\begin{aligned} \mathcal{D} &= \{\cos(j\Psi t), j \in [0, N_d]\} \cup \{\sin(j\Psi t), j \in [1, N_d]\} \\ \mathcal{W} &= \{\cos(k\Omega t), k \in [0, N_w]\} \cup \{\sin(k\Omega t), k \in [1, N_w]\} \end{aligned}$$

The frequencies of the sinusoidal functions are $\Psi = \frac{2\pi}{365.25}$ and $\Omega = \frac{2\pi}{7}$. The number of harmonics, respectively N_w for 7-day and N_d for 365.25-day periodicity, are hyperparameters of the model.

We add to the original model the dependency on temperature, expressed in HDD, and its daily difference, by including the two features in the set of regressors. The terms related to trend and holidays are kept exactly as in the original paper.

Finally, we correct the long-term model with the consumption of the previous day to get a short-term predictor:

$$R\hat{G}D(t) = R\hat{G}D^{long}(t) \frac{R\hat{G}D(t-1)}{R\hat{G}D^{long}(t-1)}.$$

The number of harmonics N_w and N_d were tuned by minimizing the AIC/BIC values.

4.6 Technical notes on model implementation

All the models, except the toroidal one, were implemented in Python, using scikit-learn and keras; automated hyperparameters tuning exploited the GridSearchCV function of scikit-learn. All the charts in the paper are realised with either Plotly or Chartify. The toroidal model was implemented in MATLAB, as well as its hyperparameter tuning routine.

5 Performance limit

The lack of benchmarks on the specific dataset calls for different ways of assessing the goodness of our models. As shown in Section 3, temperature is the most important exogenous variable. Unfortunately, the correct temperature is not available when forecasting future RGD: only a forecast is available, affected by a small yet meaningful error, which inevitably impacts the performance of the model.

Let us assume that RGD is a deterministic function g of the temperature T and some other factors $\mathbf{x} = (x_1, x_2, \dots)$: $RGD = g(T, \mathbf{x})$. In view of the analysis and the charts presented in Section 3, it is reasonable to model the relationship between RGD and T with a piecewise linear function, while the dependence on other factors can be an arbitrarily complex function \bar{g} :

$$RGD = g(T, \mathbf{x}) = \bar{g}(\mathbf{x}) + \alpha \max(T_c - T, 0) + \beta$$

Let us now suppose to perfectly know \bar{g} and the parameters α , β and T_c . Yet, the correct temperature T must be replaced with the temperature forecast \hat{T} , which is affected by a stochastic additive error ϵ , with zero mean and variance σ_ϵ^2 , such that $\hat{T} = T + \epsilon$. We can now define $R\hat{G}D$ the optimal forecast of RGD , given the temperature forecast \hat{T} :

$$R\hat{G}D = g(\hat{T}, \mathbf{x}) = \bar{g}(\mathbf{x}) + \alpha \max(T_c - \hat{T}, 0) + \beta$$

We want now to compute the mean squared error of $R\hat{G}D$. In order to simplify the derivation, we will assume that there is no error on the choice of the piece of the max function to consider. This assumption is not fulfilled, but the error introduced is not relevant, as it applies only when T is close to T_c , that is when RGD is quite low.

With this assumption, we can derive the conditional variance of $R\hat{G}D$:

$$\begin{aligned} \text{Var}[R\hat{G}D \mid T \geq T_c] &= \text{Var}[\bar{g}(\mathbf{x}) + \alpha \cdot 0 + \beta] = 0 \\ \text{Var}[R\hat{G}D \mid T < T_c] &= \text{Var}[\bar{g}(\mathbf{x}) + \alpha(\hat{T} - T_c) + \beta] = \alpha^2 \text{Var}[\epsilon] = \alpha^2 \sigma_\epsilon^2 \end{aligned}$$

Since ϵ is unbiased, it holds that $\mathbb{E}[R\hat{G}D] = RGD$. Thus:

$$\begin{aligned} \mathbb{E}[(R\hat{G}D - RGD)^2] &= \text{Var}[R\hat{G}D] = \\ &= P(T < T_c) \text{Var}[\hat{g} \mid T < T_c] = P(T < T_c) \alpha^2 \sigma_\epsilon^2 \end{aligned}$$

This last equation provides an estimate of the mean squared error due to the forecasting error on the temperatures, thus a lower bound to any modelling error.

To find a numeric value for the bound, we first estimate $P(T < T_c)$ by computing the ratio between the number of samples where $T < T_c$ is verified and the total number of available data, then we compute α through a least square fit and finally we estimate σ_ϵ^2 as the variance of the difference between the temperature forecast and the actual values. The results are shown in Table 2.

6 Analysis and Results

As mentioned in section 2, available data range from 2007 to 2017. To ensure that all samples can include RGD and temperature at similar day, the first year was discarded.

Four test sets were defined, each exactly one year long, covering 2014, 2015, 2016 and 2017. To each of them, a training set was associated, spanning from the beginning of 2008 to the day before the start of the test set. Thus, training sets cover the years 2008-2013, 2008-2014, 2008-2015, 2008-2016. In the following, we will refer to both training and test set using the year covered by the test set - thus, we will write "training set 2016" to indicate the third training set, spanning from 2008 to 2015.

On each test set, the performance of each of the five models is measured using the Mean Absolute Error (MAE).

$$MAE = \frac{1}{M} \sum_{j=1}^N |RGD_j - R\hat{G}D_j|$$

where $R\hat{G}D$ represent the forecast for RGD. MAE is preferred over MAPE due to the highly unstationary behaviour of the series, where errors in the cold months may be heavier than errors in the warm periods. Moreover, MAE is proportional to the monetary loss sustained by energy companies because of errors in nomination due to inaccurate forecasts.

Model performance is also compared to the theoretical limit derived in section 5. As the performance limit poses a lower bound to the mean squared error, the Root Mean Square Error (RMSE) is used as a metric in this context.

6.1 Hyperparameters

All the five models we considered include hyperparameters. Most of them were automatically optimized using line and grid search with cross-validation.

For ridge regression, we chose a set of 50 possible values for the regularization parameter λ , ranging from a minimum of 10^{-4} to a maximum of 50 by logarithmic steps. We opted for logarithmic rather than linear steps in order to better scan low values. Nevertheless, the line search performed on training sets 2016 and 2017 selected the minimum possible value of λ , thus highlighting that regularization is not required for RDG, given the relatively large amount of available training samples. Using training sets 2014 and 2015, we obtained different yet small *lambda*, respectively equal to 0.028 and 0.236.

For KNN we optimized the number of neighbours, in a set from 1 to 30, and the weighting strategy, choosing between uniform and inverse of distance. We obtained 9 neighbours for training set 2014, 7 for 2015 and 6 for the two remaining ones. In each set, the grid search selected the "inverse of distance" weights for the average.

The maximization of marginal likelihood for the GP model selected $\nu = 3/2$, $l = 10$ and an hyperparameter of the White kernel equal to 10. Such results are stable among all training sets.

For what concerns the toroidal model, the minimization of AIC and BIC led to the choice of $N_w = 3$ and $N_d = 1$ for each training set.

For ANN, we chose the architecture with 24-12-4-1 neurons, the ReLu activation function, the Adaptive Moment Estimation (ADAM) optimizer and the Mean Squared Error (MSE) loss function. On the other hand, we chose by a grid search a learning rate of 0.001, a number of epochs of 1000 and a batch size of 32, being the sets of possible values, respectively, $\{0.1, 0.01, 0.001\}$, $\{300, 500, 1000\}$ and $\{16, 32, 64\}$.

6.2 Parameters

By analyzing the magnitude of ridge regression parameters, we can investigate the relative importance of each feature. Results are fairly consistent among training sets.

The most relevant factor is the RGD at day before ($t - 1$), which accounts for about 45% of the sum of all weights. The second most important feature is the forecasted HDD (at time t), with 15%, followed by the RGD at the similar day ($sim(t)$), with 11%. Then, under 10%, there are RGD at $sim(t - 1)$ and the HDD of the day before ($t - 1$), both with about 6%.

Among calendar features, dummy variables for Monday and Saturday weight 3% and 2%, respectively, while all the other regressors show lower percentages. This last evidence has an interesting interpretation. Monday and Saturday are the first working day and the first non-working day of the week: thus, they are the ones where the RGD at day before alone is not adequate to catch the RGD level.

6.3 Results

In order to compute the performance limit, we used actual measures provided by Meteologica. Unfortunately, data were only available for 2015, 2016 and 2017. Results are shown in table 2 and compared with the out-of-sample RMSE achieved by the five models. The performance limit is about 2 MSCM, whilst all the models but KNN present an almost double RMSE. KNN achieves a poorer performance, with an RMSE of about 8 MSCM.

Considering the three years, ANN is the best model, closely followed by GP: both achieve a quite stable RMSE, just above 4 MSCM. The Toroidal model is also a good performer, except for the year 2015, where its error gets higher. The Ridge regression shows a slightly higher but very stable error.

If we abandon the performance limit and we focus on the comparison between models, we can switch to MAE and add also the test set 2014. Out of sample results are shown in Table 3. Overall, GP is the best performer, achieving a MAE of 2.56 MSCM, lower than the one of ANN by 0.05 MSCM. Third, but only slightly worse than ANN, is the toroidal model, while ridge regression has an average MAE about half a million of standard cubic meters greater. KNN is again the worst model, with a MAE of 5.81 MSCM.

By comparing the classification based on MAE with the one based on RMSE, we can notice slight differences, due to the different error metrics. In case of perfectly Gaussian errors, the ratio between MAE and RMSE is known to be $\sqrt{2/\pi} \sim 0.8$. However, if we compute such a ratio for each model, we get lower results: about 0.61 for GP and Torus, 0.65 for KNN and ANN and 0.71 for Ridge. This is explained by the "fat tails" of the error distributions, highlighted in Fig. 10.

Due to the seasonal behaviour of RDG, it may be of interest to study the monthly errors. In Table 4 we show the average of the absolute errors achieved by each model in each month, throughout the four test sets. It is clear that GP is the best performer during the summer period, especially from May to September, whereas in the other months ANN is more accurate. This leads us to the conclusion that the GP model is better at capturing the effects of the weekly seasonality, while ANN can better take into account the non-linear effect of temperature, mostly relevant during the cold months.

As mentioned before, to the best of our knowledge, there are no benchmarks in the literature for the task we performed. However, Zhu et al. [19] performed short-term forecasting of UK demand. Performances are still not completely comparable, for two

main reasons: first, the authors considered the whole UK demand, and not only the residential demand; second, UK climate is colder and less variable than the Italian one. Nonetheless, we can use a relative error metrics, such as Mean Absolute Percentage Error (MAPE), to try and compare model performances only on 6 cold months (from October to March). Our best model in terms of MAPE, the ANN, achieves a 3.15% MAPE, while Zhu's false neighbours filtered-support vector regression local predictor (FNF-SVRLP) reaches a 3.88 % MAPE on the 6 months.

Model	year 2015	year 2016	year 2017
Ridge	4.67	4.39	4.31
GP	4.33	4.28	4.14
KNN	7.82	8.05	8.72
Torus	5.31	4.32	3.93
ANN	4.34	4.11	3.64
Physical limit	2.15	2.02	1.98

Table 2: Yearly Root Mean Squared Error (RMSE) on test sets and performance limit

Model	year 2014	year 2015	year 2016	year 2017	Average
Ridge	3.20	3.34	3.15	3.00	3.17
GP	2.46	2.65	2.58	2.56	2.56
KNN	6.94	5.39	5.42	5.48	5.81
Torus	2.38	3.18	2.66	2.54	2.69
ANN	2.58	2.76	2.68	2.43	2.61

Table 3: Yearly Mean Absolute Error (MAE) on test sets

Month	Ridge	GP	KNN	Thorus	ANN
1	5.48	5.24	11.31	5.85	5.06
2	4.71	4.66	9.37	5.31	4.5
3	4.7	5.09	9.55	4.32	5.1
4	3.61	3.13	8.85	2.95	3.13
5	2.5	1.24	2.96	1.49	1.25
6	1.46	0.5	2.24	1.04	0.67
7	1.14	0.35	1.18	0.46	0.51
8	2.23	0.7	5.05	0.93	1.08
9	1.9	0.36	1.25	0.47	0.74
10	2.27	1.63	3.91	1.87	1.89
11	3.26	3.56	6.83	3.34	3.18
12	4.87	4.39	7.41	4.36	4.29

Table 4: Monthly Mean Absolute Error (MAE) on test sets



Figure 10: Out-of-sample model residuals in 2017

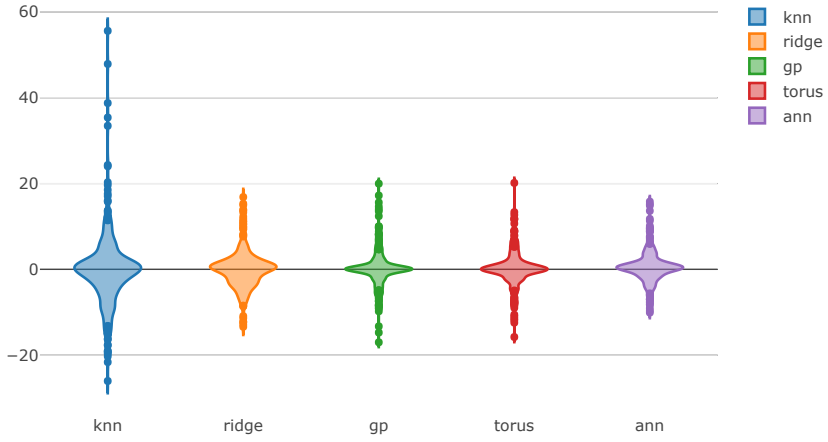


Figure 11: Distribution of out-of-sample residuals in 2017

7 Conclusion

In this paper, we faced the task of forecasting one-day-ahead the daily Italian residential gas demand. We presented the main features of the time series and its covariates, such as temperature, and the most relevant steps of preprocessing and feature extraction. Then, we described and compared five different statistical learning models:

Ridge regression, Gaussian Processes, K-nearest neighbour, Artificial Neural Networks and a Toroidal model.

As no benchmark was available for the specific task, we derived a theoretical performance limit, based on the inaccuracy of meteorological forecasts, which was then used as the ultimate benchmark for the models. Our best model, in terms of RMSE, the deep neural network, achieves an error which is about double with respect to the performance limit. On the other hand, looking at the MAE such as error measure, the GP is the best model. From the analysis of monthly performance, we realize that GP model is more accurate in following the weekly seasonality, the predominant effect in the summer period, while the deep neural network can better take into account the non-linear influence of temperature, whose contribution is greater during the winter period.

References

- [1] Abramowitz, M., Stegun, I.A., 1965. Handbook of mathematical functions: with formulas, graphs, and mathematical tables. volume 55. Courier Corporation.
- [2] Azadeh, A., Asadzadeh, S., Ghanbari, A., 2010. An adaptive network-based fuzzy inference system for short-term natural gas demand estimation: uncertain and complex environments. *Energy Policy* 38, 1529–1536.
- [3] Brabec, M., Konár, O., Pelikán, E., Malý, M., 2008. A nonlinear mixed effects model for the prediction of natural gas consumption by individual customers. *International Journal of Forecasting* 24, 659–678.
- [4] DEMİREL, Ö.F., Zaim, S., Çalışkan, A., Özuyar, P., 2012. Forecasting natural gas consumption in istanbul using neural networks and multivariate time series methods. *Turkish Journal of Electrical Engineering & Computer Sciences* 20, 695–711.
- [5] Gil, S., Deferrari, J., 2004. Generalized model of prediction of natural gas consumption. *Journal of energy resources technology* 126, 90–98.
- [6] Goodfellow, I., Bengio, Y., Courville, A., 2016. Deep Learning. MIT Press. URL: <http://www.deeplearningbook.org>.
- [7] Guerini, A., 2016. Long and short term forecasting of daily and quarter-hourly electrical load and price data: a torus-based approach , xxx.
- [8] Hastie, T., Tibshirani, R., Friedman, J., 2009. The Elements of Statistical Learning: Data Mining, Inference, and Prediction, Second Edition. Springer Series in Statistics, Springer New York. URL: <https://books.google.it/books?id=tVIjmNS30b8C>.
- [9] Murphy, K., Bach, F., 2012. Machine Learning: A Probabilistic Perspective. Adaptive Computation and Machi, MIT Press. URL: <https://books.google.it/books?id=NZP6AQAAQBAJ>.
- [10] Panapakidis, I.P., Dagoumas, A.S., 2017. Day-ahead natural gas demand forecasting based on the combination of wavelet transform and anfis/genetic algorithm/neural network model. *Energy* 118, 231–245.
- [11] Potočnik, P., Thaler, M., Govekar, E., Grabec, I., Poredoš, A., 2007. Forecasting risks of natural gas consumption in slovenia. *Energy policy* 35, 4271–4282.
- [12] Rasmussen, C., Williams, C., 2006. Gaussian Processes for Machine Learning. Adaptative computation and machine learning series, University Press Group Limited. URL: <https://books.google.it/books?id=vWtwQgAACAAJ>.

- [13] Šebalj, D., Mesarić, J., Dujak, D., 2017. Predicting natural gas consumption—a literature review, in: 28th International Conference " Central European Conference on Information and Intelligent Systems".
- [14] Soldo, B., 2012. Forecasting natural gas consumption. *Applied Energy* 92, 26–37.
- [15] Soldo, B., Potočnik, P., Šimunović, G., Šarić, T., Govekar, E., 2014. Improving the residential natural gas consumption forecasting models by using solar radiation. *Energy and buildings* 69, 498–506.
- [16] Szoplik, J., 2015. Forecasting of natural gas consumption with artificial neural networks. *Energy* 85, 208–220.
- [17] Taşpinar, F., Celebi, N., Tutkun, N., 2013. Forecasting of daily natural gas consumption on regional basis in turkey using various computational methods. *Energy and Buildings* 56, 23–31.
- [18] Tonković, Z., Zekić-Sušac, M., Somolanji, M., 2009. Predicting natural gas consumption by neural networks. *Tehnički vjesnik* 16, 51–61.
- [19] Zhu, L., Li, M., Wu, Q., Jiang, L., 2015. Short-term natural gas demand prediction based on support vector regression with false neighbours filtered. *Energy* 80, 428–436.